Korean J. Chem. Eng., 40(6), 1297-1308 (2023)
DOI: 10.1007/s11814-022-1362-2

pISSN: 0256-1115
eISSN: 1975-7220

Hydrodynamics and particles mixing in rectangular spouted bed with different base geometries using CFD-DEM

Mohammad Karimi Zand and Maysam Saidi†

Mechanical Engineering Department, Faculty of Engineering, Razi University, Kermanshah, Iran
(*Received 24 June 2022 • Revised 27 October 2022 • Accepted 30 November 2022*)

Abstract−A numerical study on the flow field and particle mixing behavior in spouted beds with the aim of considering different base shapes was carried out using CFD-DEM modeling. Four spouted beds with different base angles of 180, 120, 90 and 60 degrees were compared. In order to have a qualitative and quantitative analysis on the mixing behavior, particle tracing and Lacey mixing index calculation were executed for the models. Rectangular spouted beds generate dead-zones in the corners of the system that causes less ultimate mixing index value. As the base angle decreases, the mixing index tends to increase. A mixing degree of the case with 180 degrees base angle reaches no more than 79% at the end of the simulation, which is the lowest, whereas a mixing degree of the 60 degrees base angle reaches the maximum value of 97%, which is the highest. Particle tracing conducted in these models indicates that this matter is due to the observed fact that with more incline of the base walls, particles slip more into the spout, thus entering the circulating flow. The results also indicate this increase in the slope has almost no effect on the rate which the mixing index reaches its maximum value.

Keywords: CFD-DEM, Hydrodynamics, Inclined Base Walls, Mixing, Rectangular Spouted Bed

INTRODUCTION

Fluidized beds and spouted beds are used in numerous industrial applications due to their distinctive features. These applications include, but are not limited to, particle drying, fast pyrolysis, coating and fast freezing of particulate foods [1]. While these systems are applicable to different types of particles, spouted bed are specially used for Geldart D particles [2] which are also called spoutable particles. As a matter of fact, spouted beds were invented to overcome the defects of fluidized beds when used with coarse particles, as these particles when used in a fluidized bed, are prone to slug generation. These slug bubbles are considered as an interruption to the flow regime, since they prevent a uniform bed expansion. Large bubble generation and slug formation is a waste of gas momentum as it works as a sudden burst inside the system, rather than aerating and expanding all of the particles inside the bed [3,4]. The spouted bed flow regime is well-known for its cyclic flow pattern of particles [5,6]. This circulative flow behavior allows for better particle mixing. The mixing of particles is important since it affects the overall performance of the system, inasmuch as efficient mixing avoids generating hot zones in processes that include thermal exchange between the particles and the spouting fluid [7]. Also, efficient mixing is essential for uniform coating of pharmaceutical particles [8].

The overall dynamic conditions of spouted beds, which includes the mixing behavior of particles, is affected by the bed geometry, fluid properties (such as gas density and inlet velocity) and solid properties (particle diameter, packed bed height, particle density, etc.) [1,5]. Studies on the mixing characteristics have been conducted in the recent years regarding different aspects of these systems. Zhang et al. studied the effect of particle size on the mixing characteristics of a rectangular spout-fluid bed [9], effect of particle density [10] and the effect of inlet gas velocity of the main spout and the background fluidizing air [7]. Another research studied the effect of differing particle diameters in a binary particle mixture [11]. Renzo et al. studied a system of binary mixture with analyzing the effect of different particle densities of the binary mixture [12]. Saidi et al. studied the effect of inlet gas velocity frequency on the mixing and segregation characteristics of a pulsed fluidized bed [13,14]. Ren et al. [15] investigated the effect of particle density on the mixing behavior of a conical spouted bed. Chen et al studied the effect of annular gas inlet on solids circulation behavior in a circulating fluidized bed. In this paper, geometrical characteristics of a draft tube were also investigated [16]. Wang et al. studied the effect of superficial gas velocity on particle flux and hydrodynamics in a circulating fluidized bed downer reactor [17]. Studies on different geometrical aspects of these systems that affect the mixing behavior are present in the extensive literature, including the effect of different shapes of baffle, or separating wall in a circulating spouted bed [16,17] while other geometrical investigations, such as the effect of base angle, are rarely found.

Recently, Batista and Béttega [6] studied the effect of cone geometry on spouted bed fluid dynamics. In their research, the dynamics of the system was evaluated using cycle time of the bed. Different angles of the cone were investigated (90, 75, 60, 45, 30, 28 degrees), and the results showed that as the angle decreases, cycle time of the bed also decreases. Yue et al. studied the effect of the cone angle and baffle shape on spout deflection in a spout-fluid bed. Their

†To whom correspondence should be addressed.
E-mail: msaidi@razi.ac.ir

study primarily focused on mitigating the spout deflection, and the base geometries that they studied were 90 and 120 degrees [3]. Lou et al. also investigated the effect of the base angle of a 2-D spouted bed on the hydrodynamics and solid temperature by modeling four different geometries with inclination angles of 30, 45, and 60 degrees [18]. Perazzini et al. examined the effect of cone angle on drying skimmed milk, comparing three different cone angles of 45, 60 and 75 degrees [19]. In these studies, the same number of solids were used for their differing cases. However, in most of the present studies, the same packed bed height was considered for the investigations, which results in different solids mass between cases since with decreasing cone angle; there will be fewer particles within the same static height [19-21]. Although in the studies mentioned above the effect of cone angle was investigated on different system properties like circulation and hydrodynamics, a quantitative and qualitative study on mixing regarding different cone angles is lacking.

Studies on mixing characteristics of spouted beds have been conducted experimentally and numerically. Experimental procedure is a great tool for visual observation of particle behavior. Zhang et al. used a new method to investigate the mixing of a spout fluid bed [22]. They implemented microwave heating on the heat absorbent tracer particles in a spout fluid bed and then captured their real time trajectory using infrared camera to investigate the mixing characteristics of the system. Nevertheless, an experimental procedure is expensive compared to numerical simulation. The numerical methods used for simulating these systems, being two-fluid model and discrete element method, are also widely used. Among these two models, discrete element method is best suitable for studying these two-phase systems and specially investigating their mixing behavior, since in contrast to the two-fluid model, it provides detailed information about the particle dynamics like real time particle position that is essential in calculating the mixing index. The CFD-DEM method has been proven accurate and beneficial in the extensive literature. As a verifying example, Link et al. [1] published their results regarding a comparison between experimental and CFD-DEM study that confirmed the reliability of the CFD-DEM. Wang and Shen also studied the gas-solid flow and heat transfer of a char combustion process in a bubbling fluidized bed using a CFD-DEM approach with particle size polydispersity and thermochemical sub-models. Their model validation and results demonstrated the applicability and high potential of the CFD-DEM method [23]. As mentioned in this section, a study that specifically concerns particle mixing characteristics comparison between spouted beds with different base angles and the hydrodynamics that directly influence this matter is rarely found in the extensive literature. For this reason, a detailed CFD-DEM investigation on the mixing behavior has been performed in this study. Due to the lack of detailed analysis on the effect of geometry on mixing behavior of spouted beds, emphasis was put on the effect of the base angle on the mixing. To conduct a quantitative study on the mixing in the spouted bed, Lacey mixing index was chosen and calculated for the systems; and in order to have a qualitative comparison, particle tracing was executed to visualize the mixing state of the systems. In addition, several aspects of hydrodynamics of the systems were also analyzed with regards to the mixing behavior. Results indicate that base angle decrease has positive impact on mixing characteristics of the systems.

MATHEMATICAL MODEL

1. Governing Equations for CFD-DEM Modeling

A CFD-DEM was utilized for this study. The model used is the same model originally developed by Hoomans et al. in 1996 [24]. Two methods are at hand for simulating the contact forces between particles: Hard sphere and soft sphere. In the latter model the particles as deforming objects can be modeled by a spring and dashpot, whereas the former model assumes the particles as rigid solids that have momentary contact. The soft sphere model was chosen for this study [1,22,25].

Dynamics of each particle is tracked in a Lagrangian frame and obeys the Newtonian equation of motion:

$$m_p\frac{dv_p}{dt}=-V_p\nabla p+\frac{V_p\beta}{\varepsilon_p}(\mathbf{u}_f-\mathbf{v}_p)+m_p\mathbf{g} \tag{1}$$

The β sign is the momentum transfer coefficient due to drag. The drag model used in this equation is the same model implemented by Hoomans et al. [24] and Kawaguchi et al. [26], namely the Gidaspow model, that is a combination of the Ergun and Wen & Yu equations. The Ergun equation is developed for dense flows and low porosities (ε_f<0.8) and the equation is written as following:

$$\beta_{Ergun}=150\frac{\varepsilon_p^2\mu_f}{\varepsilon_f d_p^2}+1.75\varepsilon_p\frac{\rho_f}{d_p}|\mathbf{u}_f-\mathbf{v}_p| \tag{2}$$

The Wen & Yu equation is used for dilute flows and high porosities (ε_f>0.8):

$$\beta_{Wen\text{-}Yu}=\frac{3}{4}C_D\varepsilon_p\frac{\rho_f}{d_p}|\mathbf{u}_f-\mathbf{v}_p|\varepsilon_f^{-1.65} \tag{3}$$

C_D is the drag coefficient for an isolated spherical particle given by Schiller and Naumann (1933). This model, when used with the Gidaspow model, proves better agreement with experimental results [5]:

$$C_D=\begin{cases}\frac{24}{Re_p}(1+0.15Re_p^{0.687}) & \text{if } Re_p<1{,}000\\ 0.44 & \text{if } Re_p\geq 1{,}000\end{cases} \tag{4}$$

Whereas

$$Re_p=\frac{\varepsilon_f\rho_f|\mathbf{u}_f-\mathbf{v}_p|d_p}{\mu_f} \tag{5}$$

The gas phase is treated as a continuum in the Eulerian frame and is computed via the volume averaged Navier-Stokes equation:

$$\frac{\partial}{\partial t}(\varepsilon_f\rho_f)+\nabla\cdot(\varepsilon_f\rho_f\mathbf{u}_f)=0 \tag{6}$$

$$\&\frac{\partial}{\partial t}(\varepsilon_f\rho_f\mathbf{u}_f)+\nabla\cdot(\varepsilon_f\rho_f\mathbf{u}_f\mathbf{u}_f)=-\varepsilon_f\nabla p-\nabla\cdot(\varepsilon_f\tau_f)-\mathbf{S}_p+\varepsilon_f\rho_f\mathbf{g} \tag{7}$$

Since the spouting gas in this simulation is air at 20 °C, it is assumed to obey the general rule of a Newtonian fluid. Thus the viscous stress tensor τ_f would be:

$$\tau_f = -\left[\left(\lambda_f - \frac{2}{3}\mu_f\right)(\nabla \cdot \mathbf{u}_f)\mathbf{I} + \mu_f((\nabla \mathbf{u}_f) + (\partial \mathbf{u}_f)^T)\right] \quad (8)$$

The sink term $\mathbf{S}_p$ is given by:

$$\mathbf{S}_p = \frac{1}{V_{cell}} \sum_{Vi \in cell} \frac{V_i \beta}{\varepsilon_p}(\mathbf{u}_f - \mathbf{v}_i)\mathrm{D}(\mathbf{r} - \mathbf{r}_i) \quad (9)$$

This is the term that enables the two-way coupling for this two-phase system.

The fluid flow for this simulation is considered to be laminar, because of the large size of the particles. Although flow around the spout can be turbulent, particles are hardly affected by these turbulent fluctuations due to their inertia, i.e., velocity fluctuations are mostly damped because of the presence of the particles [1].

The porosity is calculated by the conventional way Hoomans et al. [24] introduced in their work. The equation is given by:

$$\varepsilon_{f,\,cell} = 1 - \frac{1}{V_{cell}} \sum_{\forall i \in cell} f^i_{cell} V^i_p \quad (10)$$

In this equation, f^i_{cell} is the volume fraction of particle i present in a cell. This method is the most straightforward way to calculate the porosity inside an Eulerian grid cell and works well when the cell volume is significantly greater than the particle volume [1].

NUMERICAL PROCEDURE

1. Model Verification and Grid Independency

The modeling was performed by employing the open source OpenFOAM software in addition to Fortran coding for postprocessing data. The initial step was verification of obtained results using the same pseudo-2D spout-fluid setup in Link et al. [1]. Fig. 1 represents the geometrical structure of the bed. The main spouting gas is injected via the middle inlet. Background gas (also called as fluidizing gas) is inserted via the remaining surface of the bottom pane to the two sides of the spout inlet. The height, width, and depth of the bed is 750 mm, 150 mm, and 15 mm, respectively. The width of the spout inlet is 10 mm, so the width of the background gas inlet would be 70 mm×2. A number of 24750 glass particles, same as what was used in Link et al. [1] was used in the simulation. Details of particle properties are listed in Table 1.

Boundary conditions and case setup for the validation are also equivalent to the research paper mentioned. For this initial setup, the case A of Link et al. [1] was used as simulation setup. According to this case, the spouting and background gas inlet velocities are 30 m/s and 1.5 m/s, respectively. The top plane boundary condition is exit to the atmosphere and the side planes represent the walls of the bed. Details of the case setup are listed in Table 2.

Table 1. Particle properties

Property	Value	Unit
d_p	2.5	mm
ρ_p	2,526	kg/m^3
Particle no.	24,750	-
$e_{n\,p\,to\,p}$	0.97	-
$e_{n\,p\,to\,w}$	0.97	-
$\mu_{p\,to\,p}$	0.10	-
$\mu_{p\,to\,w}$	0.10	-
$\beta_{0\,p\,to\,p}$	0.33	-
$\beta_{0\,p\,to\,w}$	0.33	-

Table 2. Validation case setup

Property	Value	Unit
Spouting gas velocity	30	m/s
Fluidizing gas velocity	1.5	m/s
ρ_g	1.2	kg/m^3
Pressure	101,325	Pa
Gas viscosity	1.8×10^{-8}	P s

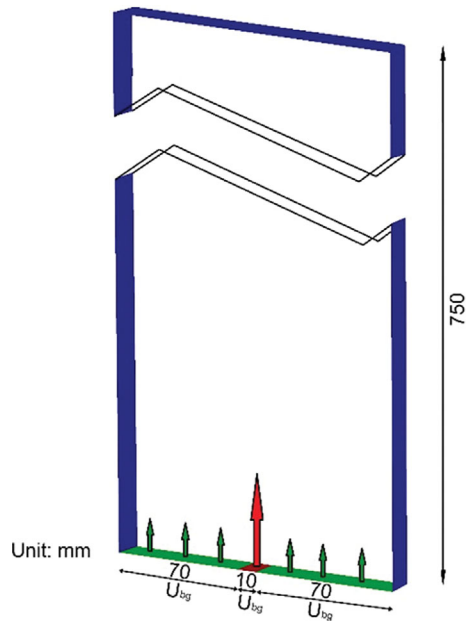

Fig. 1. Schematic view of the bed used in validation.

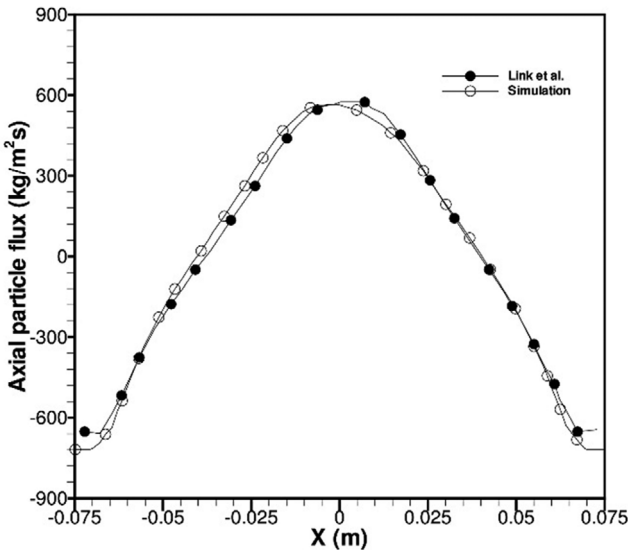

Fig. 2. Time - averaged particle flux comparison.

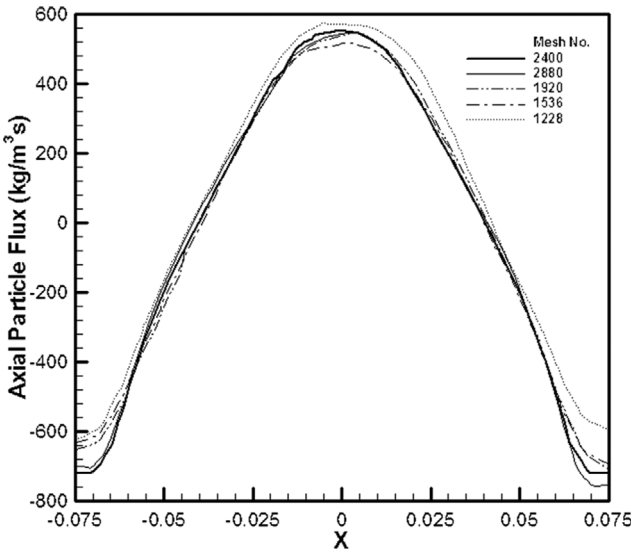

Fig. 3. Grid independence test.

The results were verified via comparing the simulation data corresponding to particle flux at z=130 mm with that of Link et al. [1]. It can be seen in Fig. 2 that the plot extracted from the simulation is comparable to the plot of the mentioned article.

Prior to modelling the systems and validating the simulation results, a grid independence test was carried out to determine the optimum mesh number that was sufficiently accurate for modelling the systems. A grid independence test was conducted for the spout-fluid bed system that was studied in the work of Link et al. [1]. First, a coarse grid was defined to model the system with 1228 meshes, and the grid was refined by 20% step by step. The mean axial particle flux was reported to evaluate the grid independency. At 2400 mesh number, the results showed a plausible accuracy, which had a less than 2% difference with the 20% finer grid. The results are shown in Fig. 3.

Table 3. Simulation setup of each case

Case	U_{sp}	U_{bg}	Unit
180^0	51	0	m/s
120^0	51	0	m/s
90^0	51	0	m/s
60^0	51	0	m/s

2. Case Setup

In this research the hydrodynamics and mixing behavior in spouted beds with different bed geometry were compared. The first case, a conventional flat bottom spouted bed, was selected as the base condition. To create it, the case used in the verification was selected. The air flow of the background fluidizing gas was transferred to the main spouting gas so that the overall air flow in the system would be identical to the initial validation setup and the simulation setup of Link et al. [1]. As mentioned in Table 2, the inlet velocity for the background air is 1.5 m/s. The surface which this air is inserted from is 70 mm×15 mm×2. By calculating this air flow then transferring it to the spout inlet, which has a surface of 10 mm×15 mm, an additional velocity of 21 m/s would be added to the spout inlet velocity. This spout inlet velocity was fixed and used throughout all case setups. To solve each case in ten seconds, around five days of run time was needed using a system with an Intel core-i7 930 CPU.

Cases 2 to 4 represent tapered spouted beds. Since the aim of this research was to investigate the effect of base angle on the hydrodynamics and mixing behavior, each of the cases of 2, 3 and 4 has a specific bottom base angle. Details of the setups of each case are listed in Table 3 and the graphical representation of each case is shown in the Fig. 4.

The collision parameters of these cases were the same as the

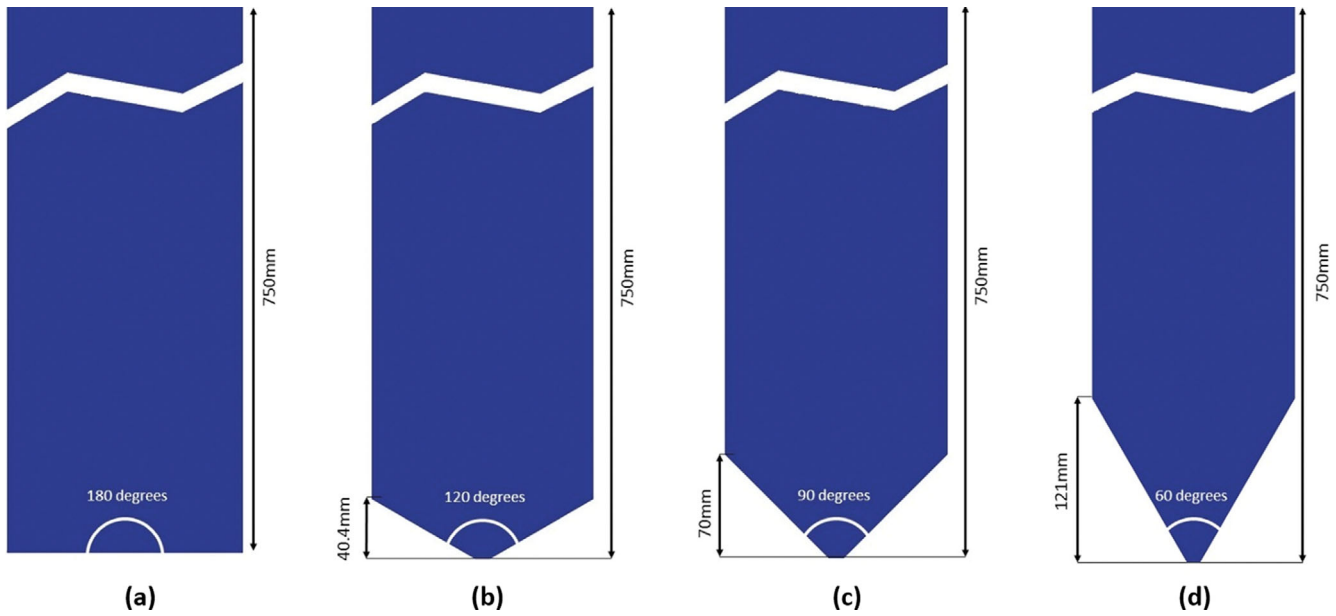

Fig. 4. Schematic view of the geometries studied (a) 180 degrees, (b) 120 degrees, (c) 90 degrees, (d) 60 degrees base angle.

Table 4. Static bed height of the cases

Case	Hs	Ums
	m	m/s
180^0	0.13	23
120^0	0.1489	24.62
90^0	0.1627	25.73
60^0	0.1825	27.25

case used for verification. As mentioned in Table 3, to have a legitimate comparison, the same number of particles was considered for each case instead of considering the same packed bed height. This is because using an inclined wall with the packed bed height method would give a smaller number of particles for each case, and as the slope increases with less base angle, a significant number of particles would be omitted from the bed. As a result, packed bed height would differ among the cases. By increasing the packed bed height, minimum spouting gas velocity, Ums, also increases. Ums is calculated for each case using the well-known Mathur and Gishler [4] empirical expression given below:

$$U_{ms} = \left(\frac{d_p}{D_c}\right)\left(\frac{D_i}{D_c}\right)^{\frac{1}{3}}\sqrt{2gH_0\left(\frac{\rho_p - \rho_g}{\rho_g}\right)} \quad (11)$$

Table 4 reflects the packed bed height and minimum spouting gas velocity for each case.

RESULTS AND DISCUSSION

In this study, a detailed investigation and comparison between four different cases with base angles of 180, 120, 90 and 60 degrees was carried out. Later in this section, hydrodynamics, mixing degree and particle tracing of the cases are compared.

1. Hydrodynamics

Particle velocity vectors in different cases are depicted in Fig. 5. In the 180 degrees case, particles in the annulus close to the vicinity of the spout flow, tend to have directions towards the main spout flow. As a result, particles in this area are more dynamic in the whole bed. In contrast, particles residing farther away from the spout vicinity, especially in the lower parts of the bed and in corners, appear to have randomized directions that are rarely or not pointed towards the spout. Thus, these particles are almost stationary throughout the whole process, and they tend to create dead-zones in the system. These dead-zones have negative effect in the overall mixing process and system homogeneity. Further investigations of the dead-zones are in the next section.

As the base angle decreases, the results show more particles inclined towards the spout flow. With more particles slipping into the flow, more mobility is achieved throughout all particles of the system. This mobile behavior results in fewer particles stuck to the walls of the system and less dead-zone formation.

Fig. 6 shows the time-averaged air velocity vectors of the cases studied. This plot and other time-averaged plots given in this study were extracted from the simulation after the system had reached a steady state condition and 10 seconds of steady state simulation was used for the time-averaged plots. Note that effects of the initial conditions were also deleted from the time-average investigations. As it is demonstrated in the figures, in the 180 degrees case, air flow around the main spout at the bottom of the bed is directed horizontally away from the spout inlet. Although the velocity magnitude is low in these parts, this air flow direction actually pushes away the particles residing in the dead-zones from the spout flow. Thus, this kind of flow behavior, has negative effect on particle loco-

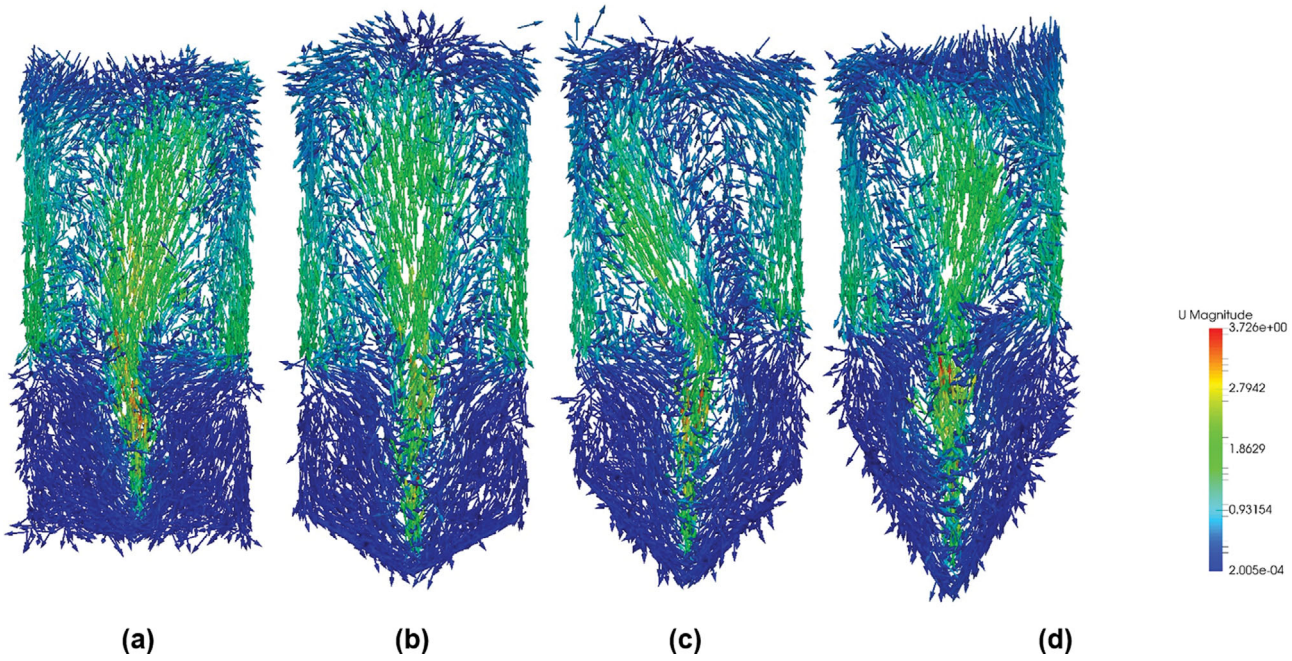

Fig. 5. Velocity vectors of particles.

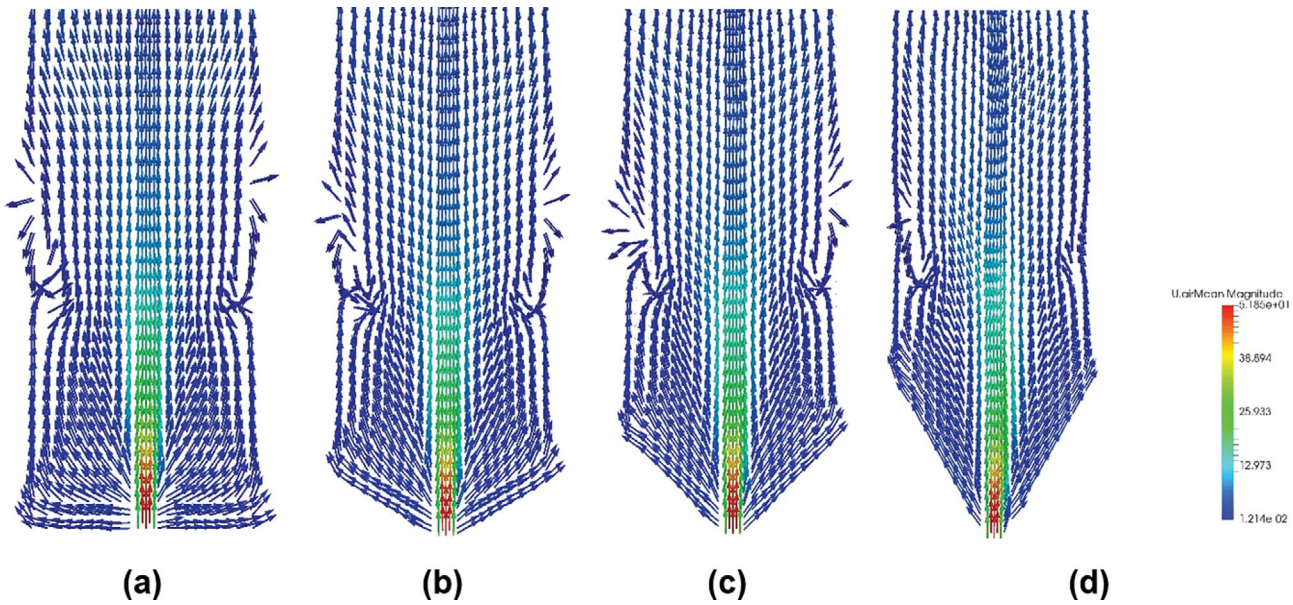

Fig. 6. Air velocity vector of the cases.

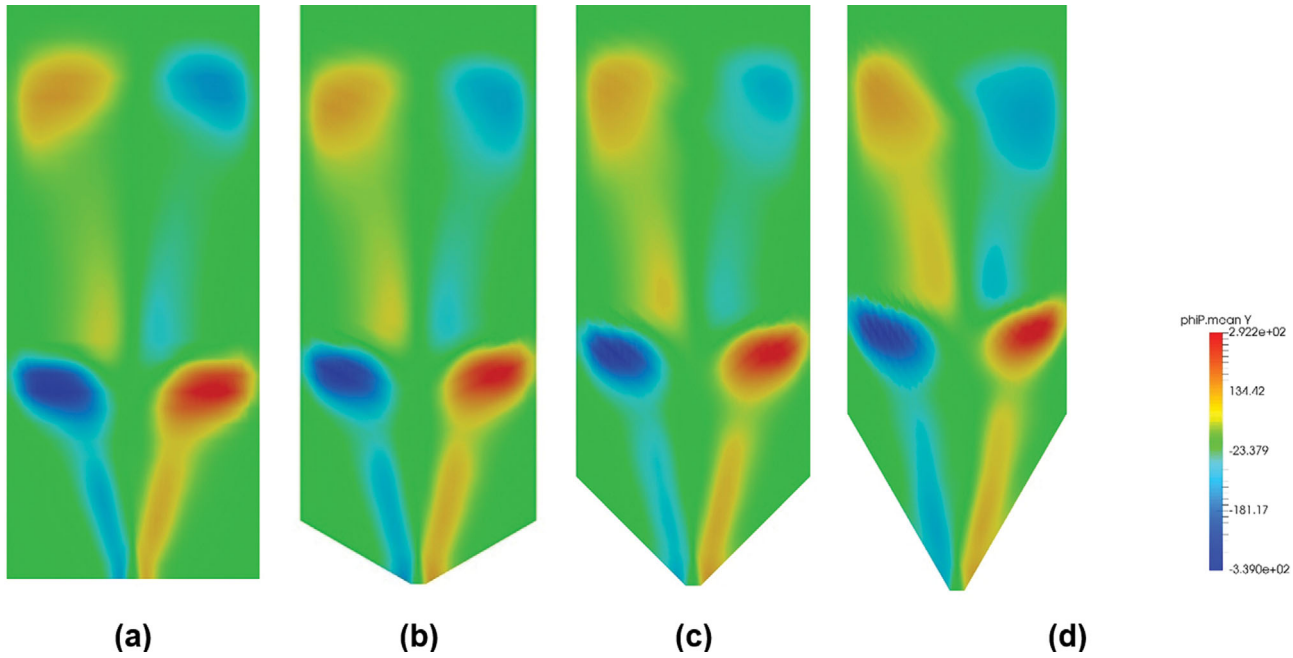

Fig. 7. Time - averaged radial particle flux.

motion, since the main mechanism that aids the particle mobility in the system, is the main spout flow. Particles need to slip from the annulus into the spout flow in order to have better mobility. Air flow velocity vector in the case of 120 degrees base angle also tends to push away the particles from transferring into the spout, since the major part of the velocity magnitude comes from the horizontal component of the velocity vector. This is because of the geometrical properties of the conical bed walls. However, as the base angle decreases, air flow velocity vectors change their direction towards a more upward orientation, resulting in less leftward and rightward thrusts among particles positioned to the left and right of the spout.

In Fig. 7 the time-averaged radial particle flux contour plots are given. The contour plots imply that there is solids mass transfer to the spout channel in the areas close to the spout flow in all cases of 180, 120, 90 and 60 degrees. Moving further away from the spout flow, solids mass transfer decreases and in the area near the walls and corners in the lower half of the beds, particle flux is near zero. As the base angle decreases, these areas with zero particle flux tend to become smaller, insofar as in the 60 degrees case there is minimal area with zero particle flux near most parts of the walls. In addition, another pattern can be seen among the cases, that in

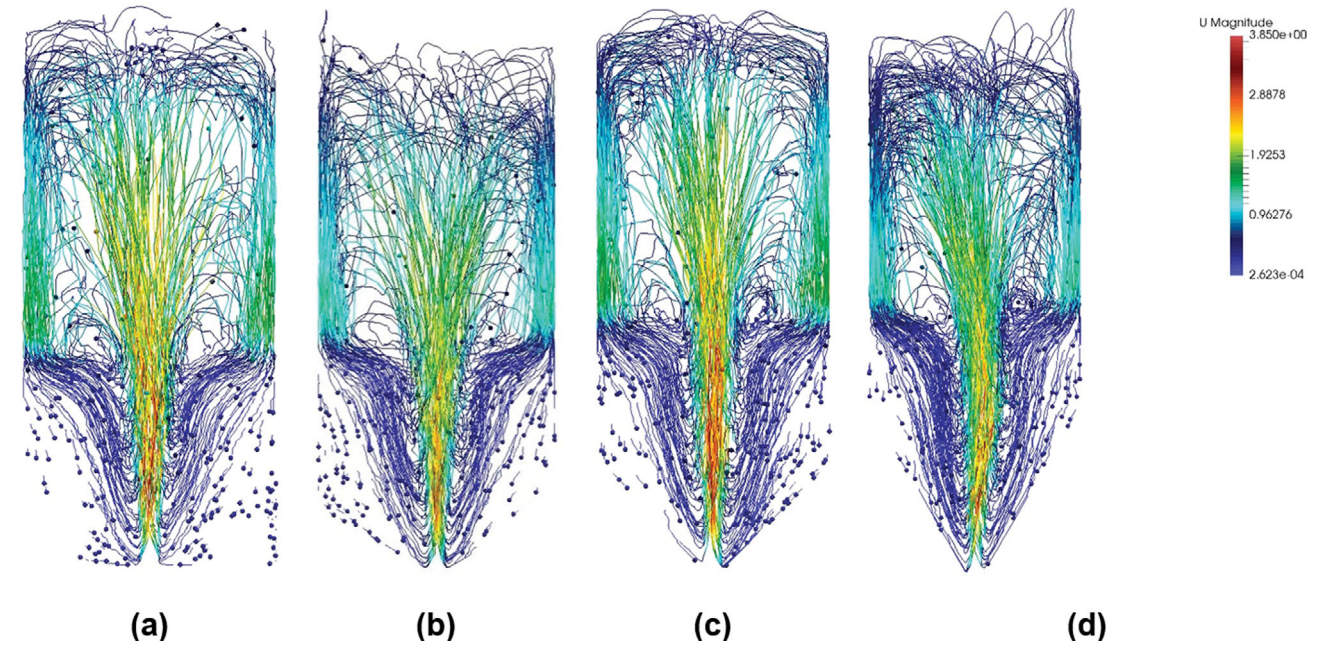

Fig. 8. Particle trajectory.

the 180 degrees case as we move downwards along the bed walls, the zero-flux zone becomes larger, and the widest area is at the bottom, whereas in other inclined cases, this is not necessarily true. As a matter of fact, the governing pattern for these other cases is that the zero-flux area is widest at the junction of the base wall and vertical wall.

Fig. 8 reflects real time particle trajectory path lines. To present a clear and less crowded plot, 247 particles were randomly chosen among all the particles scattered in the system and were tracked for 1 second in real time simulation. As can be seen in this plot, particles that are entrained by the spout flow and the circulative regime of the system posse a relatively long path line that represents the large distances they have traveled in the one second, which prompts mixing with other particles in the flow. In contrast, particles trapped in the corners of the system (dead-zones) have miniscule movement, which results in no mixing with other particles. By increasing the base angle, these areas that contain near to zero particle path line length become larger. This claim can also be proved by tracking the velocity of every particle in the system.

Fig. 9 shows the overall time averaged comparison of particle movement throughout the entire beds. In these charts, particles that have a movement velocity below an infinitesimal value are categorized as stationary particles, and other particles are divided into four motional groups with regard to their dominant direction. Cases with smaller base angle have a lower proportion of stationary particles trapped in the dead-zones. In contrast, higher number of particles have downward movement, which are mostly the particles in the annulus region. Particles that are moving towards the center of the system, namely inwards direction, have almost the same proportion of the data. The amount of particles that have upwards motion, which are the particles entrained in the spout channel, becomes slightly larger with a decrease in the base angle. Same pattern of slight increase is perceptible for the particles moving outwards from the center of the system. These outward movements can be seen at the top region of the spouted beds that the spout channel creates a fountain of particle flow. Therefore, the same slight increase becomes more recognizable since particles entrained by the spout enter the fountain last.

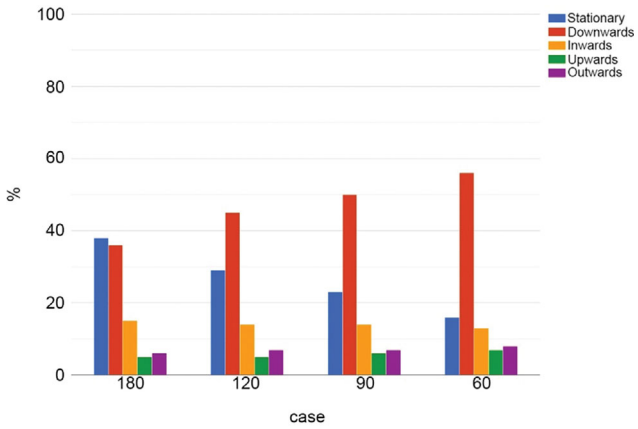

Fig. 9. Time - averaged motion directions ratio.

Next, axial particle flux is discussed using plots given in Fig. 10. Mean particle flux is plotted at different heights of 0.12 m, 0.10 m, 0.07 m and 0.04 m near the bottom of the beds, where the flux seams to vary among the cases. Fig. 10(a) represents a comparison of the particle flux between the four cases of 180, 120, 90 and 60 degrees at 0.12 m. At this height, the case of 180 degrees shows the same behavior as static height; thus, the system has a robust particle stimulation, since this height is close to its static bed height. As the base angle decreases, particle flux at the sides of the bed decreases, to the extent that for the 60 degrees case, the value is almost zero. This is expected, since as it was mentioned before, the

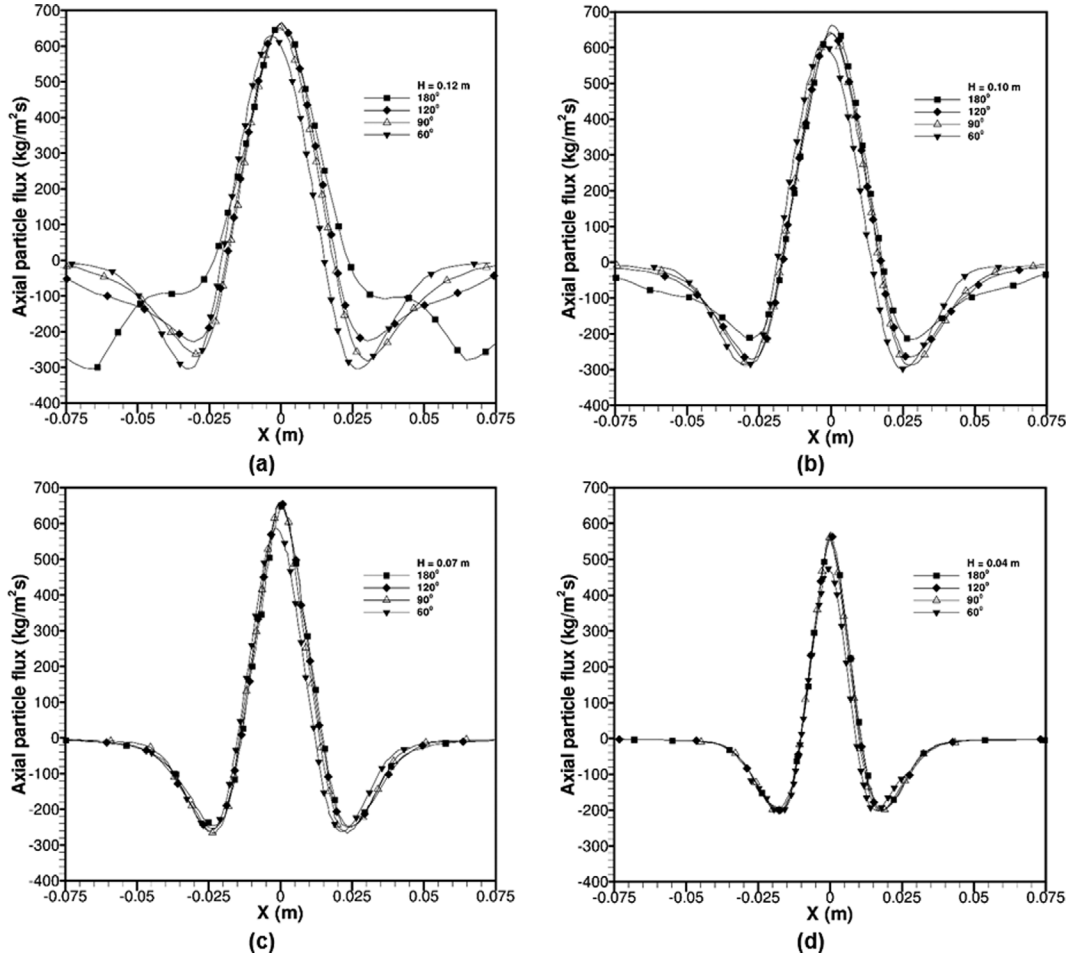

Fig. 10. Time - averaged Axial particle flux comparison at heights (a) 0.12 m, (b) 0.10 m, (c) 0.07 m, (d) 0.04 m.

cases with inclined base walls appear to have their least solids mass transfer at the whereabouts of junctions of the base wall and the vertical wall. In the 60 degrees case, this junction is located at the height of 0.1212 m. In the other cases of 90 and 120 degrees, we also have more mobility among particles, since their plots have non-zero values. Fig. 10(b) shows the particle flux at H=0.10 m. At this height the plot for the 180 degrees case still has not reached the values near zero and the dead-zones of the system. The cases of 120 and 90 degrees start to flatten at the sides, meaning this is where the dead-zones start to form. The case of 60 degrees, on the other hand, has a horizontally shorter plot. This is because the geometry of the system is narrower compared to the other cases. In addition, the domain which the plot has zero value is shorter compared to the other cases.

Fig. 10(c) illustrates the particle flux plot at the height of 0.07 m that is the junction height for the 90 degrees case. At this height, all of the cases appear to have reached the dead-zones, and a wide domain of the plots have flattened out, having values near zero. In contrast, the 60 degrees case shows infinitesimal to no flattening at the sides, and has values slightly lower than zero. This means that at this point dead-zones no longer are present, and solids mass transfer is being done in the system. Next, Fig. 10(d) shows the particle flux at the height of 0.04 m, which is again near the 120 degrees case junction at 0.0404 m. The flat zero value area for the cases of 180 and 120 degrees has grown larger, meaning more particles are stuck in the dead-zones to the sides of the system. The 60 degrees case plot has become shorter in horizontal length, this is again due to the geometry of the bed. This plot shows no values of zero at the sides of the system. Thus, dead-zones are not effective at this part. The 90 degrees case also starts to cut off at the edges, as the height is at the narrowing part of the system. In this case, the zero flattened area has become shorter, meaning dead-zones have become smaller. To conclude the analysis on the flux plots, in the conventional 180 degrees case, dead-zones become larger as we move towards the bottom of the bed. By giving incline to the bottom walls of the system, the dead-zones are cut off, resulting in less particles stuck to the sides of the system, and never entering the circulating flow of the bed.

2. Mixing Characteristics

For a deeper understanding of the mixing behavior, quantitative degree of mixing was calculated for each case. Several means have been introduced for statistical analysis of particulate mixing. Wen et al. published a comparative study on different mixing index calculation methods [27]. Among the mixing indices introduced, Lacey mixing index [28] is the most used due to its ease of application and suitable index-time curve, that is valued between 1 and

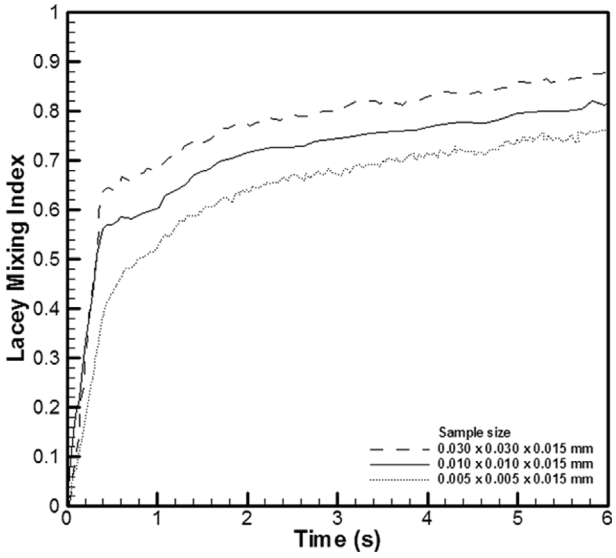

Fig. 11. Sample size effect investigated for the 180 degrees case.

0. The index-time curve being valued this way facilitates the comprehension of the mixing of the system. Hence, lacey mixing index was chosen and calculated for the system geometries. The formulae of calculating this index are given later on in this section. This method basically clusters the particles into a binary group by a neutral property, say by coloring a fraction of the total particles and then tracing them in the system. Calculation of this index requires the bed to be divided into N multiple samples. As discussed by Ren et al. [15], the Lacey mixing index depends on the sampling size. The lacey mixing index simply considers the tracer particle concentration variance in each sample in comparison with the whole tracer particle concentration. The effect of the sample size was investigated to select a plausible sample size, and the results are illustrated in Fig. 11. As shown in Fig. 11, an excessively large sample yields a higher mixing index, which may incorrectly indicate that the mixed state of the system is better than the actual condition of the system. As an example, consider that we take only one sample from the bed and its volume is equal to the whole bed size. As this sample includes all of the particles of the system, the tracer particle concentration in this sample is equal to the overall tracer particle concentration. This leads to zero variance, which results in a fully mixed index. In contrast, an extremely small sample size would cause excessive mixing index plot fluctuations and irrational results, in addition to giving out a smaller mixing value.

Therefore, samples of identical volume were taken from the bed, each having dimensions of 10 mm×10 mm×15 mm. In addition, we attempted to define the sample size so as not to have samples that contain both normal and tracer particles at the beginning of the lacey mixing index calculation, as this will cause a mixing plot with an initial mixing value higher than zero. Fig. 12 shows a schematic of the samples taken from one of the cases (60 degree case).

The concentration of the tracer particles is then considered in each sample. After that, the variance of the concentration of each sample as compared to the total average tracer concentration is calculated. In this study, half of the particles in each system were

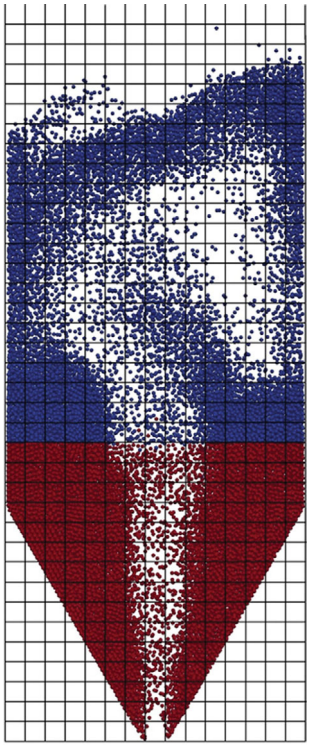

Fig. 12. Schematic of samples taken from the system.

colored. Therefore, the total average concentration of the systems, denoted by $\overline{P}$, is 0.5; the variance, S^2, is calculated by:

$$S^2 = \frac{1}{N}\sum_{i=1}^{N}(P_i - \overline{P})^2 \tag{12}$$

As mentioned, N is the number of samples taken from the bed. P_i is the local concentration of tracer particles in a sample. A completely mixed bed would have a variance of S_r^2. The subscript r denotes the state of being randomized and fully mixed. For a system with given total average concentration of tracer particles S_r^2 could be calculated using the following equation:

$$S_r^2 = \frac{\overline{P}\times(1-\overline{P})}{n} \tag{13}$$

where, n is the possible number of particles in a sample. In addition, variance of a completely segregated mixture is shown by S_0^2 and is calculated by:

$$S_0^2 = \overline{P}\times(1-\overline{P}) \tag{14}$$

At last, the degree of mixing is defined by M, and the formula is given by:

$$M = \frac{s_0^2 - s^2}{s_0^2 - s_r^2} \tag{15}$$

Since S^2 represents a mixing state between the states of fully mixed and fully segregated, and its value is between S_r^2 and S_0^2, the mixing degree M of a given binary mixture at any time would be a number between 1, fully mixed, and 0, fully segregated. In that manner, lacey mixing index can clearly demonstrate the state of mixing of the system.

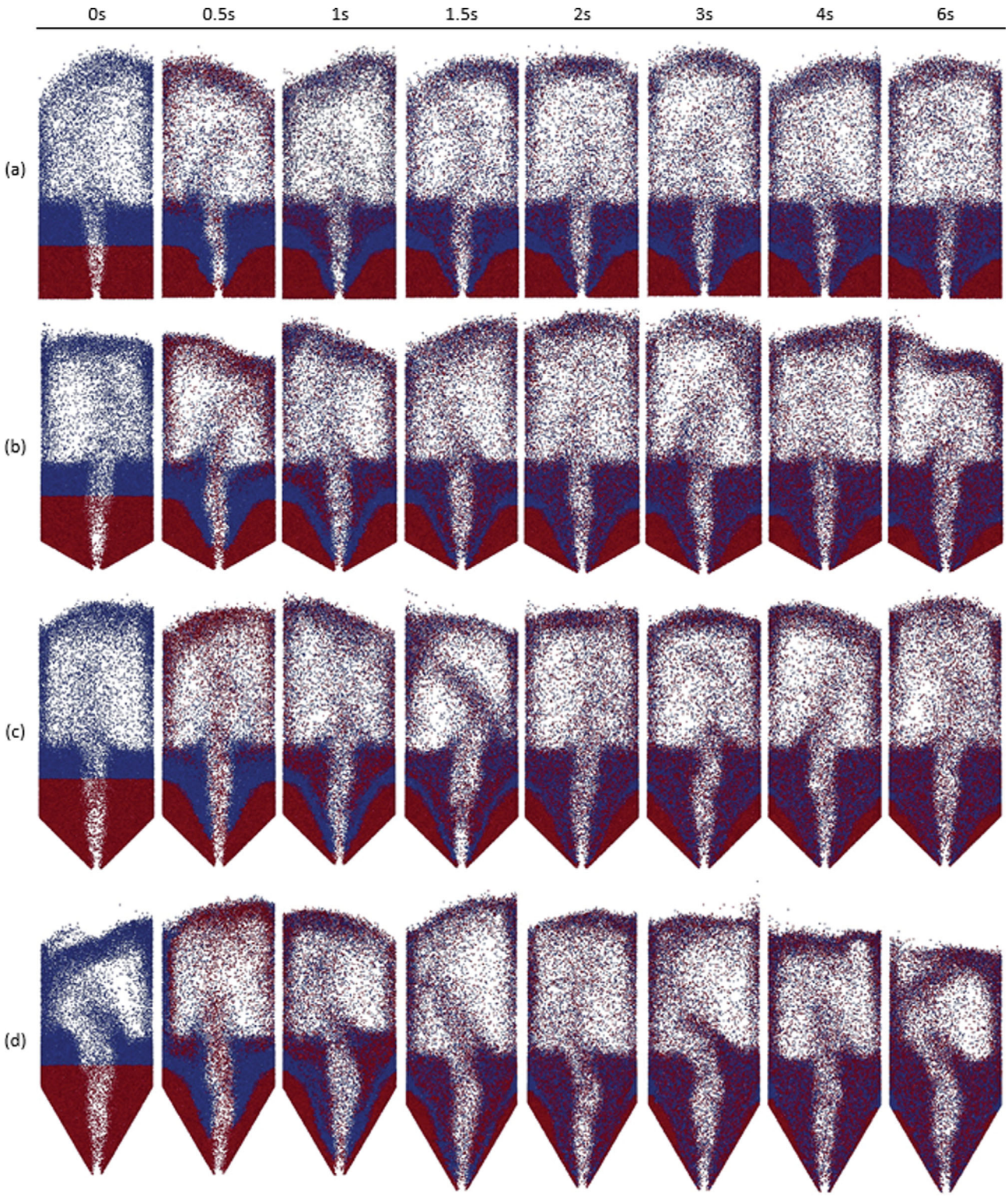

Fig. 13. Real - time particle tracing comparison.

In addition to the mixing index, real-time graphical illustration of particle tracing of the spouted beds was also carried out in this study. The focus of particle tracing was to illustrate the formation of the dead-zones in each geometry. In each case, at the time when the spouted bed reached a steady state operating condition, the lower half of the particles were colored in red. After that, they were traced throughout the bed. Snapshots of this particle tracing were taken from each system and compared in Fig. 13.

As shown in the figures, dead-zones are created in the bottom of the bed to the left and right side of the spout. The particles in

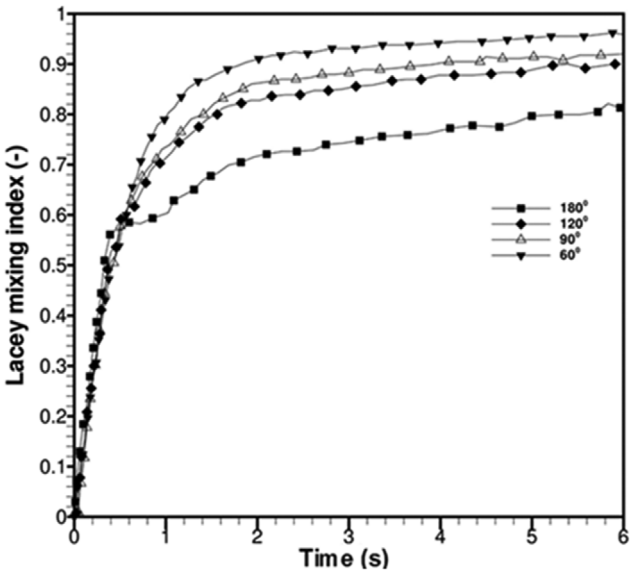

Fig. 14. Lacey mixing index comparison.

these zones have minimal movement compared to the rest of the particles in the system. Particles that form the dead-zones tend to be stationary and do not get involved in the mixing process, resulting in poor mixing behavior of the system and less mixing degree. As the angle decreases, the size of the dead-zones also decreases. Dead-zones formed in the rectangular spouted bed are more "stubborn" compared to other geometries. Even after 6 seconds of simulation, a major part of the dead-zones remains segregated. In contrast, dead-zone formation in the geometry with 60 degrees base angle shows the least stability, to the extent that after 6 seconds of simulation only a minimal part of the tracer particles remains stuck to the base walls. Thus, as the angle decreases, base walls get more inclined and more particles tend to slip into the spout flow, resulting in more mixing of particles and improved mixing characteristics.

Quantitative results of Lacey mixing index calculation are also shown in Fig. 14. This plot demonstrates the comparison of the mixing indices between the geometries. As shown in the mixing index plot, with the decrease of angle, the mixing index increases, meaning that the overall mixing behavior of the system has improved. These results comply with the particle tracing discussed previously. Meaning that the smaller number of particles stuck in the dead-zones, the more maximum value of mixing degree.

Another feature that stands out in this plot is that the initial speed of the mixing index appears to be the same among the cases. This issue has been investigated in the extensive literature, and conclusions gather around the same opinion that the initial speed which the mixing degree time-index curve of spouted beds reach, the maximum degree of mixing is only related to the velocity of the air inlet [7,17,27-31].

Finally, note that the minimum spouting gas velocity is increasing throughout the cases because of the geometries that affect the packed bed height. As mentioned in the previous sections, the same spout inlet velocity was used for all the cases. This means that for the cases with less base angle, Usp/Ums would be less. Thus, if equal values of Usp/Ums were to be used, the results would change slightly for the better.

CONCLUSIONS

The mixing characteristics of spouted beds were investigated in this study. Using these simulation conditions, four cases of conical spouted beds with base angles of 180, 120, 90 and 60 degrees were analyzed and compared in order to study the effect of geometry on mixing behavior of these systems. In all cases, mixing behavior was studied at the systems equilibrium, and the effects of initial transient unsteadiness were omitted from the data. Mixing was examined through different aspects. Dynamic behavior was examined by particle flow, air flow and analysis of particle flux at different parts of the bed. Lacey mixing index was chosen for quantitative calculation of the mixing degree of the systems. In addition, to have a qualitative examination of the mixing, particle tracing was conducted for the systems. Following results were concluded from this work:

1) Spouted beds are prone to form dead-zones by accumulation of particles in the lower corners of the system that result in less particle interaction with the flow and circulation, therefore less mixing degree.
2) Base angle is effective in the dynamic behavior of the systems. With smaller angles, smaller dead-zones are formed in the system. Smaller angles also result in less unyielding dead-zones.
3) In contrast to flat-bottom spouted beds, dead-zones in spouted beds with inclined base walls tend to form at the junctions of the base walls and vertical bed walls.
4) Smaller angles represent better overall mixing behavior and higher mixing degree. As a qualitative way of expressing the matter at hand, tracer particles are more uniformly distributed in the bed when angle decreases.

NOMENCLATURE

Roman Symbols

C_D : drag coefficient
D : distribution function
D_c : bed diameter
D_i : inlet diameter
d_p : particle diameter
g : gravitational acceleration
H_0 : packed bed height
I : unit vector
M : lacey mixing index
m_p : particle mass
N : number of samples
n : number of particles in each sample
p : pressure
$\overline{P}$: average tracer particle concentration
P_i : tracer particle concentration in ith sample
r : position
Re_p : Reynolds number
S^2 : variance

S_r^2 : variance of totally mixed state
S_0^2 : variance of totally segregated state
$\mathbf{S}_p$: particle drag sink term
t : time
$\mathbf{u}_f$: fluid velocity
U_{ms} : minimum spouting gas velocity
v_p : particle velocity
V_p : particle volume
V_{cell} : mesh cell volume

Greek Symbols

β : momentum transfer coefficient
ε_p : volume fraction of particles
ε_f : volume fraction of fluid
μ_f : viscosity of fluid
ρ_f : fluid density
ρ_p : particle density
τ_f : fluid stress tensor
λ_f : gas phase bulk viscosity
f : volume fraction

REFERENCES

1. J. M. Link, L. A. Cuypers, N. G. Deen and J. A. M. Kuipers, *Chem. Eng. Sci.*, **60**(13), 3425.
2. D. Geldart, *Powder Technol.*, **7**, 285 (1973).
3. Y. Yue, S. Wang and Y. Shen, *Powder Technol.*, **394**, 278 (2021).
4. K. B. Mathur and P. E. Gishler, *AIChE J.*, **1**(2), 157 (1955).
5. N. Epstein and J. R. Grace, *Spouted and Spout-Fluid Beds*. (2011).
6. J. N. M. Batista and R. Béttega, *Dry. Technol.*, **40**(10), 2073 (2022).
7. Y. Zhang, B. Jin, W. Zhong, B. Ren and R. Xiao, *Chem. Eng. Res. Des.*, **88**(5-6), 757 (2010).
8. L. A. P. de Freitas, *Particuology*, **42**, 126 (2019).
9. Y. Zhang, W. Zhong, B. Jin and R. Xiao, *Ind. Eng. Chem. Res.*, **52**(15), 5489 (2013).
10. Y. Zhang, W. Zhong, B. Jin and R. Xiao, *Ind. Eng. Chem. Res.*, **52**(15), 5489 (2013).
11. Y. Zhang, Y. Zhao, Z. Gao, C. Duan, J. Xu, L. Lu, J. Wang and W. Ge, *Renew. Energy*, **136**, 193 (2019).
12. A. Di Renzo, F. P. Di Maio, R. Girimonte and B. Formisani, *Powder Technol.*, **184**(2), 214 (2008).
13. M. Saidi, H. Basirat Tabrizi, J. R. Grace, C. J. Lim and G. Ahmadi, *Ind. Eng. Chem. Res.*, **54**(32), 7933 (2015).
14. M. Saidi, H. Basirat Tabrizi, S. Chaichi and M. Dehghani, *Powder Technol.*, **264**, 570 (2014).
15. B. Ren, Y. Shao, W. Zhong, B. Jin, Z. Yuan and Y. Lu, *Powder Technol.*, **222**, 85 (2012).
16. G. Zhang, Z. Chen, J. Bao, W. Wei and X. Bi, *Can. J. Chem. Eng.*, **99**(11), 2294 (2021).
17. C. Wang, J. Zhu, X. Lan, J. Gao and S. Barghi, *Powder Technol.*, **301**, 848 (2016).
18. K. Luo, J. Lin, S. Wang, C. Hu and J. Fan, *Chem. Eng. Technol.*, **42**(11), 2310 (2019).
19. M. T. B. Perazzini, F. B. Freire, M. C. Ferreira and J. T. Freire, *Dry. Technol.*, **36**(3), 341 (2018).
20. Y. Yue, C. Zhang and Y. Shen, *Chem. Eng. Sci.*, **230**, 116234 (2021).
21. M. Fang, K. Luo, S. Yang, K. Zhang and J. Fan, *Ind. Eng. Chem. Res.*, **52**(22), 7556 (2013).
22. Y. Zhang, W. Zhong and B. Jin, *Powder Technol.*, **208**(3), 702 (2011).
23. S. Wang and Y. Shen, *Chem. Eng. Sci.*, **240**, 116655 (2021).
24. B. P. B. Hoomans, J. A. M. Kuipers, W. J. Briels and W. P. M. V. A. N. Swaaij, *Chem. Eng. Sci.*, **51**(1), 99 (1996).
25. I. Estiati, H. Altzibar, M. Tellabide and M. Olazar, *Powder Technol.*, **316**, 87 (2017).
26. T. Kawaguchi, M. Sakamoto, T. Tanaka and Y. Tsuji, *Powder Technol.*, **109**(1-3), 3 (2000).
27. Y. Wen, M. Liu, B. Liu and Y. Shao, *Procedia Eng.*, **102**, 1630 (2015).
28. P. M. C. Lacey, *J. Appl. Chem.*, **4**(5), 257 (2007).
29. B. Jin, Y. Zhang, W. Zhong and R. Xiao, *Ind. Eng. Chem. Res.*, **48**(22), 10055 (2009).
30. S. Parvathaneni and V. V. Buwa, *Powder Technol.*, **372**, 178 (2020).
31. T. Oschmann, J. Hold and H. Kruggel-Emden, *Powder Technol.*, **258**, 304 (2014).